Journal of Fluorescence (2023) 33:239–253
https://doi.org/10.1007/s10895-022-03075-1

RESEARCH

A DFT Study on New Photovoltaic Dyes to Investigate their NLO Tuning at Near Infrared Region (NIR) as Pull–push Effect by End Capped Acceptors

Abrar U. Hassan[1] · Sajjad H. Sumrra[1] · Muhammad F. Nazar[2] · Cihat Güleryüz[3]

Received: 2 August 2022 / Accepted: 4 November 2022 / Published online: 18 November 2022

Abstract

Throughout the opto-electronic devices industry, organic materials with considerable nonlinear optical (NLO) capabilities are being used. By employing 4,6-di(thiophen-2-yl)pyrimidine as a standard molecule, a series for new dyes (**DMBMB1-DMBMB6**) are created in the present paper by altering their functionalization with various electron acceptor (A) functional groups. The density functional fheory (DFT) and time dependent DFT (TD-DFT) based calculations have been performed to explore NLO responses by adjustment of different A units. The energy gap (E_{gap}) of their highest occupied molecular orbitals (HOMOs) and lowest unoccupied molecular orbitals (LUMOs) was ranged between 0.22–2.43 eV which was also used to calculate their global chemical parameters (GRPs). All the new dyes were subjected to UV–Vis studies revealing their frequencies being red shifted from starting dye (**DMBMB**). The theoretical investigations like frontier molecular orbital (FMO) and natural bond orbital (NBO) analysis was used to investigate their intramolecular charge transfer (ICT). The dye **DMBMB6** had the greatest linear polarizability, first hyperpolarizability (α_{total}), and second order hyperpolarizability (β_{total}) for all the developed dyes. In conclusion, due of their low ICT, all the dyes showed potential NLO features. Scientific researchers would be able to harness these NLO features to discover NLO materials for current and future uses.

Keywords ICT · NLO · Non-fullerene · NBO · UV–Vis studies

Introduction

The organic dyes are most encouraging classes of fluorescence science with outstanding photovoltaic (PV) performance in the near infrared range (NIR) [1] with better intramolecular charge transfer (ICT) [2], increased molar absorptivity [3], and tunable electrochemical attributes [4]. Furthermore, altering an appropriate aromatic or functional component in the production of fluorescent organic dyes with inter-connected electronic systems is a great way to change their absorption (λ_{max}) and/or emission wavelengths [5]. The dye sensitized solar cells (DSSCs), small molecule organic solar cells (OSCs), photodynamic treatment, chemosensory, and fluorescent probes are among their other possibilities [6]. They are particularly valuable for PV and biological applications because of these capabilities [7]. In recent years, nonlinear optical (NLO) active chromophore have attracted greater attention due to their usefulness in a variety of technology purposes [8]. Most of the organic based frameworks have a broad E_{gap}, are NLO active [9], and offer a quick reaction time [10]. They have also been widely modified for optical storage devices [11], image interpretation [12], and photonic switching operations [13]. A comparison of organic and inorganic NLO chromophore demonstrates that organically systems offer numerous advantages over inorganic systems, including a quick reaction time [14], great molecular flexibility [15], excellent processing efficiency [15], and also a strong nonlinear (NL) polarization rate [16].

✉ Abrar U. Hassan
hassanabrar2016@gmail.com

✉ Sajjad H. Sumrra
sajjadchemist@gmail.com

[1] Department of Chemistry, University of Gujrat, Gujrat 50700, Pakistan

[2] Department of Chemistry, Division of Science and Technology, University of Education, Lahore 60700, Multan Campus, Pakistan

[3] Department of Opticianry, Altınbaş University, 34144 İstanbul, Turkey

Scientists have focused on generating organic dyes with specific architectures and electrical molecular features to attain the requisite NLO properties [17]. In organic NLO-based materials, polarization is caused by electron delocalization in the main framework [18]. The electronic transition as donor (D) → acceptor (A) via a π-linker for an efficient ICT can be achieved by modifying the chemical compositions of molecules to synthesize significant NL photonic materials [19]. As a result, organic dyes having a high interconnected electron density electronically density could be preferable species NLO materials [20]. The D and A moieties are also accountable for the requisite ground-state charge imbalance, as per the data previously published [21]. Scientists have focused on generating organic dyes with specific architectures and electrical molecular features to attain the requisite NLO properties [22]. In organic NLO based materials, polarization is caused by electron delocalization in the main framework [23]. Electrons travel toward the D via a π-linker to the receptor in an electronic structure, resulting in ICT [24]. Modifying the chemical composition to generate significant NL photonic materials is, therefore, a clever strategy [25]. As a result, organic dyes having a high interconnected electron density electronically density could be preferable species for second and third-order NLO materials [26]. The non-fullerene acceptors (NFAs) have attracted a lot of interest in the last decade [27], particularly for investigation into improving PV performances [28]. As far as light is absorbed is concerned, they have surpassed their fullerene equivalents, D → A combination diversity [29]. Because of their remarkable electron transport capacities, a large range of NFA species have been researched during the last decade for their electro- and photoelectrochemical characteristics [30]. We chose NFA dyes in this study to investigate their NLO capabilities from a theoretical point of view [31], based on these intriguing aspects of conjugated NFA molecules.

The results of NLO characteristics with the study on the title dyes have not yet been showed. Simulations relying on density functional theory (DFT) were being conducted to examine NLO characteristics to bridge the research gap [32]. Different A units have been developed by coupling various A units and conjugated π-linkers, using the NFA dyes **DMBMB1-DMBMB6** as a standard. This work is critical for calculating NLO implementations since it elucidates the effects of the D, many A units, and π-linkers in NFA dyes. The DFT and TD-DFT estimations were utilized to obtain natural bond orbital (NBO) assessment, global reactivity parameters (GRPs), frontier molecular orbitals (FMOs), densities of states (DOSs), and UV–Vis analysis for NLO properties. NFA is thought to have a significant effect in the NLO material sector.

Methodology

The present study was conducted using the Gaussian 09 software [33] using various long range [34] and range separated functional [35] at level of Density Functional Theory (DFT) [36]. The DFT related parameters like (FMO, NBO, DOS, UV–Vis and NLO properties) of newly designed D-π-D-π-A framework of dyes were systematized to calculate in chloroform at CAM-B3LYP functional with 6-31G + (d,p) basis set [37]. An FMO study was used to calculate the E_{gap}, which allows the lowest amount of energy needed for the transfer from HOMO to LUMO to be estimated. To detect hyper conjugative relationships and intra—molecular charge carrier, an NBO approach was used [38] at the same basis sets. The dispersion of energy states was found using DOS computations. To explore charge transfer, UV visible based λ_{max} was recorded [39]. The parameters of NLO characteristics like dipole moment (μ_{nor}), linear polarizability, and first and second order hyperpolarizability (α_{total} and β_{total}) values were used to define how polarizable these dyes could be for better repsonces. From output files, the findings were acquired using the Gaussview [40], Avogadro [41], as well as Chemcraft [42] programs.

While examining the GRP like Electron Affinity (EA), global electrophilicity (ω), Ionization Potential (IP), Chemical Potential ($\boldsymbol{\mu}$), electronegativity (x), global hardness (η), and global softness (σ), the E_{LUMO} and E_{HOMO} are used to depict reactivity and stability. The formulas below are used to compute various parameters using Koopmans theorem.

$$\boldsymbol{IP} = -E_{HOMO} \tag{1}$$

$$\boldsymbol{EA} = -E_{LUMO} \tag{2}$$

$$\boldsymbol{\chi} = \left(\frac{\mathbf{IE} + \mathbf{EA}}{2}\right) \tag{3}$$

$$\boldsymbol{\eta} = \frac{1}{2}[\mathrm{HOMO} - \mathrm{LUMO}] \tag{4}$$

$$\boldsymbol{\mu} = -\left(\frac{\mathbf{IE} + \mathbf{EA}}{2}\right) \tag{5}$$

$$\boldsymbol{\sigma} = \frac{1}{2\eta} \tag{6}$$

When a molecular system obtains an extra electrostatic potential via the environment, it gauges energy stability as Parr characterized it. It is a reactivity trait that enables for a quantitative categorization of ω in general.

$$\omega = \left(\frac{\mu^2}{2_\eta}\right) \tag{7}$$

Another important module that affects optical performance is their light harvesting efficiency (LHE). Charge-transfer sensitivity is strongest in dyes having a high LHE level. The LHE for dyes may be calculated using the calculation (Eq. 8).

$$LHE = 1 - 10^{-f} \tag{8}$$

The open circuit voltage (V_{oc}), being an important metric for finding the cost effectiveness of optoelectronic devices is usually computed using the equation below.

$$V_{OC} = \frac{1}{e}\left[E_{HOMO^{(D)}} - E_{LUMO^{(A)}}\right] - 0.03 \tag{9}$$

Equations (10) and (11) have been used to calculate the indicated dyes for their total polarizability/hyperpolarizability with their tensors [43].

$$< \alpha > 1/3\left(\alpha_{xx} + \alpha_{yy} + \alpha_{zz}\right) \tag{10}$$

$$\beta_{total} = \left[\left(\beta_{xxx} + \beta_{xyy} + \beta_{xzz}\right)^2 + \left(\beta_{yyy} + \beta_{xxy} + \beta_{yzz}\right)^2 + \left(\beta_{zzz} + \beta_{xxz} + \beta_{yyz}\right)^2\right]^{1/2} \tag{11}$$

Results and Discussion

The current study emphasizes on NFA organic frameworks for their PV and NLO qualities. The newly designed PV design with **D-π-D-π-A** type arrangement with chemical formula 2-(6'-(benzo[b]thiophen-2-yl)-[4,4'-bipyrimidin]-6-yl)-6-methyl-6,10b-dihydrothieno[3',2':5,6]indeno[2,1-b]indole has four segments: D-1, π-Spacer, D-2 and π-Spacer 4-methyl-3a,4-dihydrocyclopenta[b]indole (**MDI**) was used as D-1 and phenyl rings were used as π-spacers. As there was any example of such electron-rich versus electron poor systems to create a pull–push effect. So we used the D-2 as 4,6-di(thiophen-2-yl)pyrimidine which is very common PV materials. We simulated its experimental λ_{max} value with several long range and range separated functionals. Theoretically developed dyes with different A units and π-spacers generated from **MDI**-**DTB** with a **D-π-D-π** framework of dyes. The A units as 7,7′-(4,4-dimethyl-4Hsilolo[3,2-b:4,5-b′]dithiophene-2,6-diyl) (**A1**), dithiophene-2,6-diyl) (**A2**) dithiophene-2,6-diyl) dithiophene-2,6-diyl) (**A3**), dithiophene-2,6-diyl) dithiophene-2 (**A4**), bis(6-fluoro-4-(5′-methyl-[2,2′-bithiophen]-5-yl) (**A5**) benzo[c][1,2,5]thiadiazole) (**A6**) were used in the dye framework being A-2. The moiety **DTB** was used as a benchmark and its newly designed dyes **DMBMB1**-**DMBMB6** (Scheme 1). A first D moiety, second D moiety, first π-linker, second π-linker, was maintained for construction purposes in the designed dyes, but the A was (**A1**-**A6**) replaced.

The (i) NLO calculations and (ii) polarizability (iii) λ_{max} were calculated to provide insight into how various A units interacted and how fixed units impact NLO comments in response. The very first D moiety (**MDI**), second D moiety (DTB), phenyl π-linkers, and the A substituent (**A1**-**A6**) were kept for assembly purposes in the created dyes **DMBMB1**-**DMBMB6**.

FMOs Analysis

The analyzed dyes with their key quantum chemistry characteristics such as electronic parameters, molecular stabilities, electron transfer attributes, and chemical reactivity may be decided via their FMO analysis. Dyes with their kinetic stability and chemical stability are intimately related to their energy gap ($E_{gap} = E_{LUMO}$-E_{HOMO}) (Table 1). To possess fine PV possibility, the dyes that make up D-π-D-π-A must have their structure optimized to achieve a consistent orientation [44]. Their structural morphological characteristics should be monitored for because they are significant in determining the μ_{nor}, efficient packing ability, and other PV-related properties. Each of these dye-related considerations is critical for achieving their NLO results.

The electron hole pairs, ω, η, μ, and σ are all controlled by E_{gap} values as *pull–push* effect. The greater the value of polarizability, the smaller the E_{gap}, resulting in a fantastic NLO value. The energy difference (E) value of dye **DMBMB1** was 2.331 eV which is higher than the E_{gap} values. Overall E_{gap} values for all the designed dyes were noted as: **DMBMB3** (2.43) > **DMBMB1** (1.82) > **DMBMB4** (1.67) > **DMBMB5** (1.58) > **DMBMB2** (1.52) > **DMBMB6** (0.22). The D units, A units, π-spacers, and end cap A units are all engaged in the arrangement of the developed dyes, which is why their disparity in energy (E) quantities are reduced. Because to compositional changes to dye **DMBMB1** (Fig. 1). By introducing two and one chlorinated/fluorinated A species, the E_{gap} were further reduced around 1.67 and 1.58–1.67 eV in dyes **DMBMB2** and **DMBMB3** where two chloro units were shown to be more successful in lowering the E_{gap} than one chloro unit. Due to the addition of one fluoro group on the A part, the E_{gap} value in dye **DMBMB4** raised significantly to 1.67 eV.

This rise in E_{gaps} might be attributed to the fluoro group for its resonance effect being less enhanced than their chloro groups. Because the fluoro and chlorinated groups

Scheme 1 Design of new dyes (**DMBMB1-DMBMB6**) with D-π-D-π-A framework

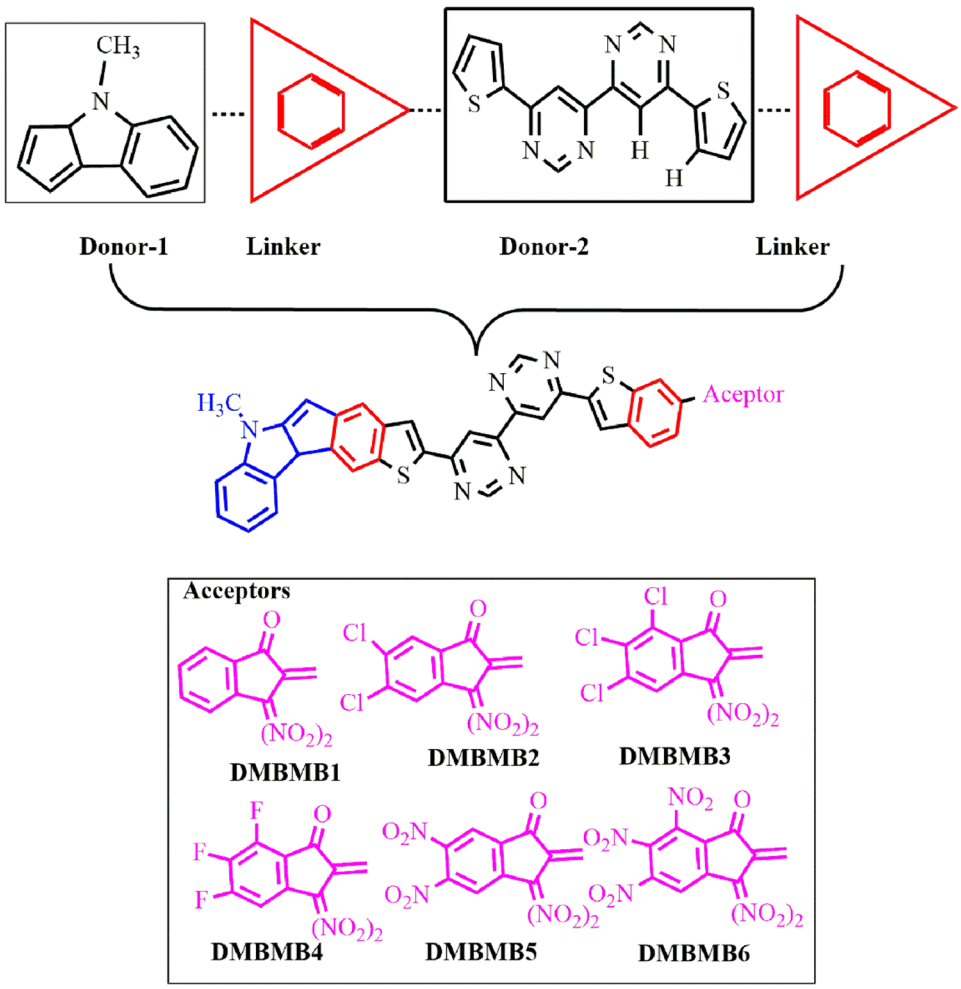

were D units owing to resonance effects, dyes **DMBMB2**, **DMBMB5** and **DMBMB6** had smaller E_{gaps}. The E_{gap} in dye **DMBMB6** was further lowered to 0.22 eV owing to nitro groups which had a significant electron withdrawing property by negative inductive activity. Due to the obvious substantial conjugation implicated in the biphenyl rings as well as the end-capped A section that has nitro units and the dye **DMBMB6** had the smallest E_{gap} among all dyes.

The existence of electronegative entities (fluoro, chloro and nitro groups) upon that A subunits can efficiently reduce electrostatic potential concentration from other regions of the A unit, decreasing their E_{gap}. An analysis of their FMOs with energy gaps showed that the dyes can execute a significant ICT phenomenon from D to A units using π-linkers. The optical gap values characterize the ICT interaction from D to A part, with the help of the π-spacer, which supplies profound insight into linked functional relationships of the NLO structures. As showed in figure, the contour portions of FMOs were used to specify the transmission of electrical charges. The LUMOs charge charge densities were only seen on the A-2 and second π-linkers over all the dyes **DMBMB1-DMBMB4**. The electronic population in the HOMO was found on first π-spacer, second D, and first A unit. First charge transfer from D to the A unit via π-linker was necessary for the NLO response activation. As a function of this impact, the dyes **DMBMB1** and **DMBMB6** may be evaluated as viable NLO candidates.

Table 1 FMO energies and their energy gaps for new dyes **DMBMB1-DMBMB6**

Dyes	E_H	E_L	E_{gap}
DMBMB1	–6.79	–4.97	1.82
DMBMB2	–7.60	–6.08	1.52
DMBMB3	–7.56	–5.13	2.43
DMBMB4	–7.41	–5.74	1.67
DMBMB5	–7.58	–6.00	1.58
DMBMB6	–6.13	–5.91	0.22

Global Reactivity Parameters

Considering GRP characteristics, the HOMO → LUMO energy difference (optical gap) is used to explain the reactivity/stability of the PV dyes. The GRPs such as

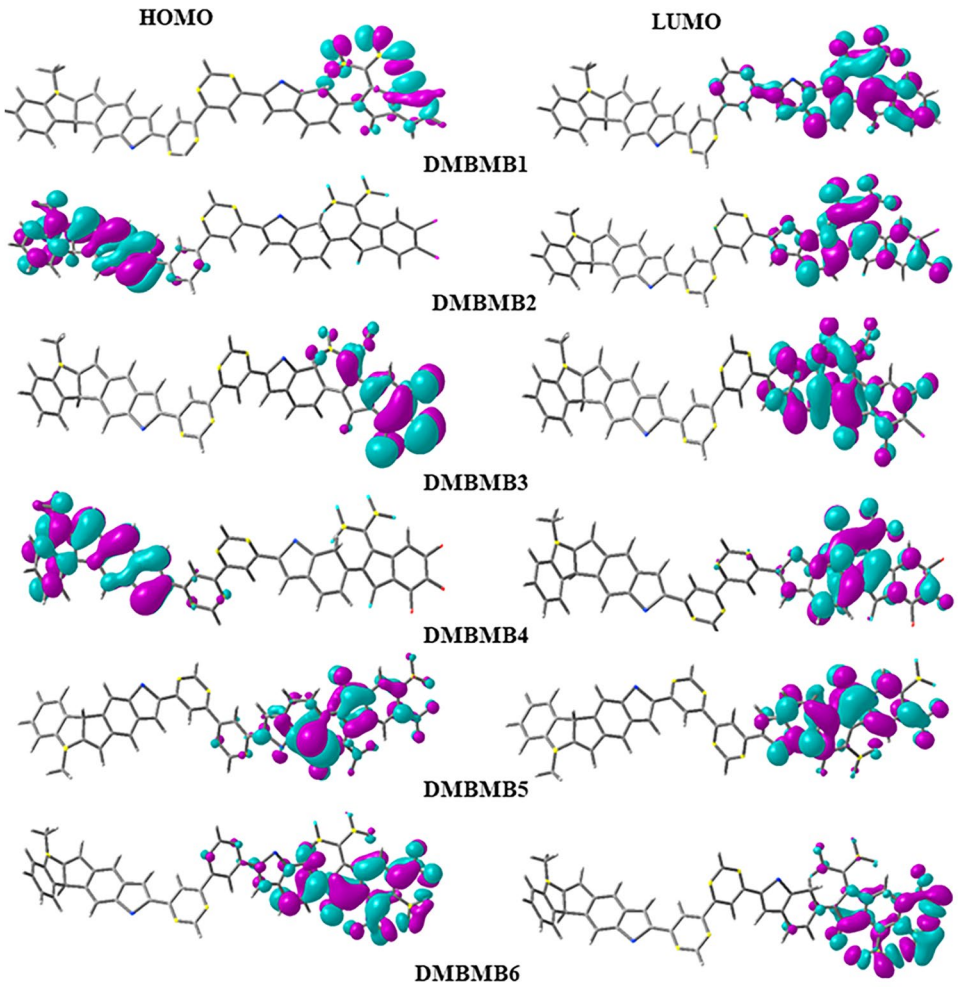

Fig. 1 FMO analysis of dyes (**DMBMB1-DMBMB6**) at B3LYP level

IP, EA, x, η, ω, μ, and σ could well be calculated using the energy gap of FMOs. The ability to give electrons is referred to as ionization potential; whereas the ability to bring electrons is referred to as x. Molecular dyes with better μ and η present better kinetic stability. These variables also have a direct association with energy gaps with equal and negative values related to σ. The overall order for μ values were noted as: **DMBMB6** (4.46) > **DMBMB2** (0.66) > **DMBMB5** (0.63) > **DMBMB4** (0.6) > **DMBMB1** (0.55) > **DMBMB3** (0.41) (Table 2).

The μ is the energy which can be acquired or generated because of a variation in the molecular density of the specified species, such as in a chemical reaction or phase transition. Their overall order was noted as: **DMBMB1** (-5.88) > **DMBMB6** (-6.02) > **DMBMB3** (-6.35) > **DMBMB4** (-6.57) > **DMBMB5** (-6.79) > **DMBMB2** (-6.84). The dye **DMBMB2** had the highest **IP** value, 7.6 eV, showing that the D moiety had efficiently transferred the electrostatic potential density to the A unit, while dye **DMBMB6** had the lowest **IP** value

Table 2 GRP analysis of dyes **DMBMB1-DMBMB6**

Comp	IP	EA	χ	μ	η	σ	ω
DMBMB1	6.79	4.97	5.88	–5.88	0.91	0.55	18.99
DMBMB2	7.60	6.08	6.84	–6.84	0.76	0.66	30.73
DMBMB3	7.56	5.13	6.35	–6.35	1.22	0.41	16.57
DMBMB4	7.41	5.74	6.57	–6.57	0.84	0.60	25.85
DMBMB5	7.58	6.00	6.79	–6.79	0.79	0.63	29.11
DMBMB6	6.13	5.91	6.02	–6.02	0.11	4.46	161.84

of 6.13 eV. The IP of all newly designed dyes, in their decreasing order as noted as: **DMBMB2** (7.6) > **DMBMB5** (7.58) > **DMBMB3** (7.56) > **DMBMB4** (7.41) > **DMBMB1** (6.79) > **DMBMB6** (6.13). Likewise, the order of their decreasing EA potential was noted as: **DMBMB2** (6.08) > **DMBMB5** (6) > **DMBMB6** (5.91) > **DMBMB4** (5.74) > **DMBMB3** (5.13) > **DMBMB1** (4.97). The μ of any species has been the energy which can be absorbed/released owing to a change in the particles density of the particular species, such as in a chemical process or phase transitions, according to thermodynamics [45]. The dye **DMBMB3** had the greatest η, which was lowered to 0.11 eV in dye **DMBMB6**.

An overall order relating their order in their descending order was seen as: **DMBMB3** (1.22) > **DMBMB1** (0.91) > **DMBMB4** (0.84) > **DMBMB5** (0.79) > **DMBMB2** (0.76) > **DMBMB6** (0.11). As compared to their η and ω values with the values in their decreasing order as: **DMBMB6** (161.84) > **DMBMB2** (30.73) > **DMBMB5** (29.11) > **DMBMB4** (25.85) > **DMBMB1** (18.99) > **DMBMB3** (16.57), examined substances had reduced σ. **DMBMB6** has the greatest value of 15.23 eV, while **DTB-MDI** has the lowest value of 11.71 eV. The growing trend of σ values was reported as dye **DMBMB** in all tested substances. Overall order for x was recorded as: **DMBMB2** (6.84) > **DMBMB5** (6.79) > **DMBMB4** (6.57) > **DMBMB3** (6.35) > **DMBMB6** (6.02) > **DMBMB1** (5.88).

NBO Analysis

An NBO investigation aids in the discovery of hydrogen bonds in designed molecules that arise from hyper conjugated interactions [46]. It gives a realistic picture for examining intramolecular delocalization and electrostatic potential density moving from the electron D units to electron requiring of the units. The interaction between the electron donating moieties becomes more important as the energy of stabilization increases. The stabilization energy formula is represented by Eq. 12 using a second-order perturbation technique.

$$E^{(2)} = q_i \frac{\left(F_{i,j}\right)^2}{\varepsilon_j - \varepsilon_i} \tag{12}$$

qi signifies electron donating orbital occupancy, while E(2) denotes stabilization energy, and $F_{i,j}$ denotes NBO Fock matrix elements that are off-diagonal, and j and i denote diagonal elements.the charge density based examination of their NBOs is an efficient procedure and useful basis for exploring conjugative CT in structural frameworks. The transition of charge in N8-C10 (π) → C7-C9 (π*) sytem was related with highest value of 22.80 kcal/mol as the most reliable transition with a dominant association of D → A (N8-C10 → C7-C9) units (Table 3). Among all transition systmes, the system with O54 (LP) → C47-C48(π*) had the lowest stabilization energy (0.65 kcal/mol). The outputs of these stabilization energies are caused by a weak contact between being a D and A units. The most notable transition displayed by dye **DMBMB5** was N56(LP) → C43-C52(π*) had its stabilization energy of 16.72 kcal/mol and O54 (LP) → C47-C48(π*) was related with lowest stabilization energy (0.65 kcal/mol). Because of resonance, all electronic transitions showed stabilization energies which had the lowest stabilization energy value of 0.11 kcal/mol in **DMBMB6** for transitions like O63 (LP) → C48-N62(π*). The findings demonstrate that delocalized antibonding orbitals, along with their electronic bonding orbitals, play a crucial role in ring stability and significant structural technology. As a matter of fact, it is reasonable to assume that the sustained conjugation observed throughout **DMBMB1**-**DMBMB6** dyes was required for stabilization.

Density of States

The fermi levels for electronic states as density of states (DOS) per unit volume per unit energy are electronic occupied orbitals with quantized energies [47]. A DOS having an unusually high value shows that multiple types of states are available per its energy levels. The absence of a state for excited electrons is represented by a zero value along the axis. DOS models may be used to calculate general dispersion of excited state because of energy and energy gap values. The newly designed dyes **DMBMB1-DMBMB6** had their DOS graphs at DFT level of theory (Fig. 2) with A group participation was 47–54% for HOMOs and 23–43% for LUMOs.

In all dyes all the D units gave 54–71% to HOMO to LUMOs for π-linkers provided 45–49% to HOMOs and 18–26% to LUMOs. Their contributions prove that the design of diverse dyes by changing distinct effective A moieties has a key influence in electronic charge cloud transmittance in various ways. Each dye is divided into three parts: a D, a π-linker and an A. The maximum charge density of the HOMO was around 6–11 eV upon that π-spacer, while the LUMO content at the donor part was 1.5 eV suggesting successful CT as D → A. The largest HOMO density seen in dye **DMBMB2** is 7.21 eV and the highest LUMO charge density was on A units, which contributes 73% of the charge. The A units limited the largest HOMO density to 7–14 eV for dye **DMBMB3** and later, while the π-spacer limits the maximum LUMO concentration to around 24 eV, increasing the electron-withdrawing nature while simultaneously extending the conjugation. All the DOS spectral analysis had

Table 3 NBO analysis newly derived dyes (**DTB1-DTB6**)

Dye	D (i)	Type	A (j)	Type	$E^{(2)}$	E(j)E(i) (au)	$F_{i,j}$ (au)
DMBMB1	C1-N2	π	C1-C7	π^*	1.22	1.14	0.033
	C1-C3	π	C1-N2	π^*	1.33	1.12	0.034
	C4-N6	π	N2-C4	π^*	2.08	1.11	0.043
	N8-C10	π	C7-C9	π^*	22.80	0.31	0.075
	N6	LP	N2-C4	π^*	5.45	0.79	0.059
DMBMB2	C1-N2	π	C7-C9	π^*	0.83	1.25	0.029
	C13-S14	π	C9-C11	π^*	1.10	1.21	0.033
	S19-C21	π	C5-C18	π^*	2.21	1.08	0.044
	C21-C22	π	C18-S19	π^*	2.31	0.95	0.042
	O64	LP	C48-N62	π^*	0.62	1.05	0.024
DMBMB3	C1-C2	π	C18-S19	π^*	1.02	0.96	0.028
	C22-C29	π	C18-C20	π^*	1.33	1.19	0.035
	C23-C24	π	S14-C16	π^*	2.17	0.88	0.039
	C28-C30	π	C21-C27	π^*	0.83	1.18	0.028
	O51		C42-C44	π^*	27.03	0.63	0.118
DMBMB4	C30-C31	π	C22-C29	π^*	1.65	1.16	0.039
	C32-N34	π	C30-C31	π^*	0.92	1.22	0.030
	O55	LP	C52-N53	π^*	19.69	0.46	0.085
DMBMB5	N34-C35	π	C31-C32	π^*	2.15	1.30	0.047
	C35-C36	π	C28-C33	π^*	0.87	1.08	0.027
	N56	LP	C43-C52	π^*	16.72	0.37	0.072
	O54	LP	C47-C48	π^*	0.65	0.71	0.021
DMBMB6	C42-C43	π	C23-C24	π^*	1.04	0.99	0.029
	C43-C52	π	C42-C43	π^*	0.62	1.17	0.024
	C45-C46	π	C42-C43	π^*	0.90	1.09	0.028
	O63	LP	C48-N62	π*	0.81	1.06	0.027

significantly support the FMO results obtained. The LHE is another important aspect that decides the optical efficiency of fluorophores in their efficiency. The higher the CT, the higher the LHE. An overall order of all the values were noted as in their descending order: **DMBMB5** (0.0011) > **DMBMB6** (0.001) > **DMBMB4** (0.0006) > **DMBMB1** (0.0036) > **DMBMB3** (0.0268) > **DMBMB2** (0.0004).

Electronic Absorbance/Emission Analysis

The ultraviolet visible (UV–Vis) spectroscopy provides further evidence for several sorts of electronic changes in the molecules [45], including λ_{max}, transition energy (E), and f^{os}. In the gaseous phase (Fig. 3), those parameters were derived using TD-DFT computations at the CAM-B3LYP/6-31G + (d,p) level to graph the representative λ_{max} shifts in the dyes **DMBMB1**-**DMBMB6** with an inverse relation between their E and λ_{max}. For same spectral assignments in chloroform (Fig. 4), the λ_{max}, f^{os}, and excitation energy (E) are computed and had λ_{max} values ranging from 711.408 to 930.247 nm with slight redshift. The λ_{max} values in nm in their decreasing order were noted as: **DMBMB5** (892) > **DMBMB2** (881) > **DMBMB6** (856) > **DMBMB3** (835) > **DMBMB4** (818) > **DMBMB1** (533).

Among the developed dyes, the reference dye **DMBMB** has the lowest λ_{max} value. The λ_{max} of the reference dye molecule obtained experimentally match the calculated findings (Table 4). The results showed that electron-withdrawing end-capped A units had a considerable impact on maximum values. The red shift in λ_{max} is caused by this electron-deficient moiety. All the dyes **DMBMB1**-**DMBMB6** had the λ_{max} wavelengths ranging from 780–930 mm, which were red shifted in comparison to **DTB**.

With lowermost E (1.33–1.44 eV), the dyes **DMBMB2** and **DMBMB6** showed a larger red shift. Charge transfer is possible because to the narrow energy gap. The dyes **DMBMB1**, **DMBMB3**, and **DMBMB4** had similar λ_{max} values, with oscillator strength (f^0) of 0.006–0.0268. The dye **DMBMB1**-**DMBMB6** had the E values of 0.77–1.66 eV, which were lower than the standard, which has E value of 1.743 eV. The computed fluorescence intensity of such pertinent dyes structures in chloroform was well given the already reported results (Fig. 5). It further suggests that in the solvent trap, the H-bond to the lone pairs of alkene unit in singlet state was ruptured by the transfer of lone pairs to

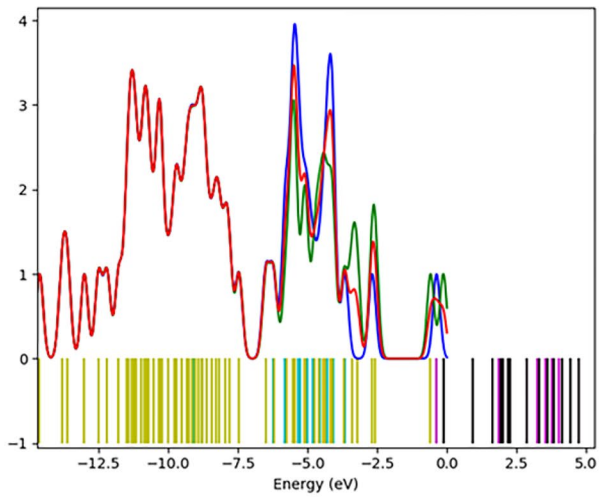

DMBMB1

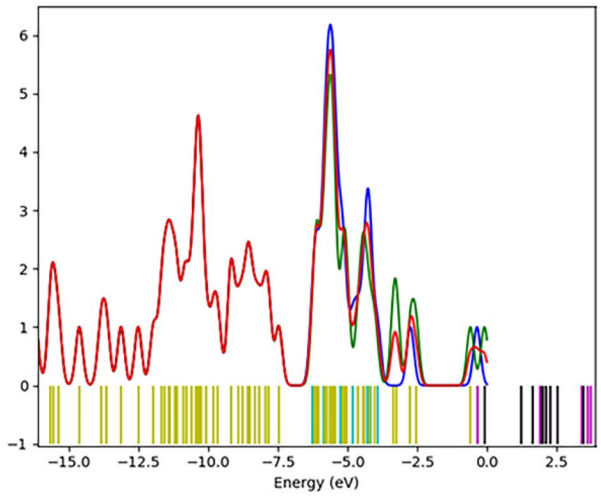

DMBMB2

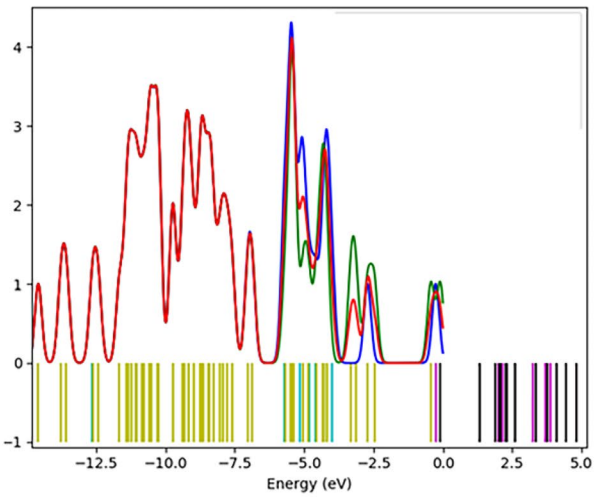

DMBMB3

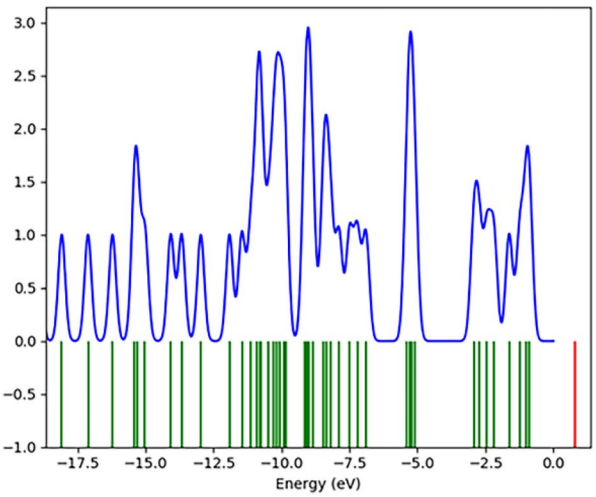

DMBMB4

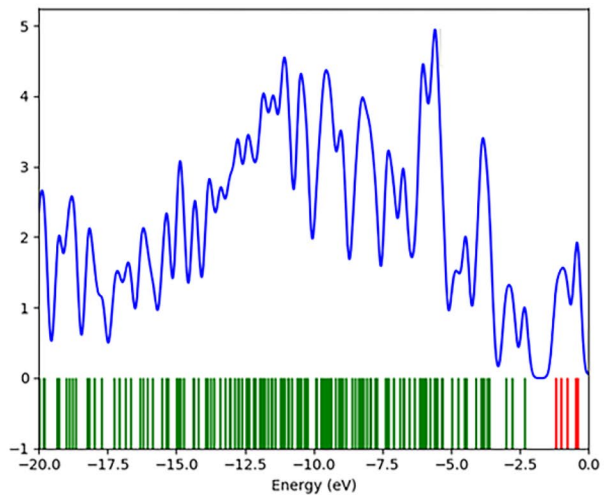

DMBMB5

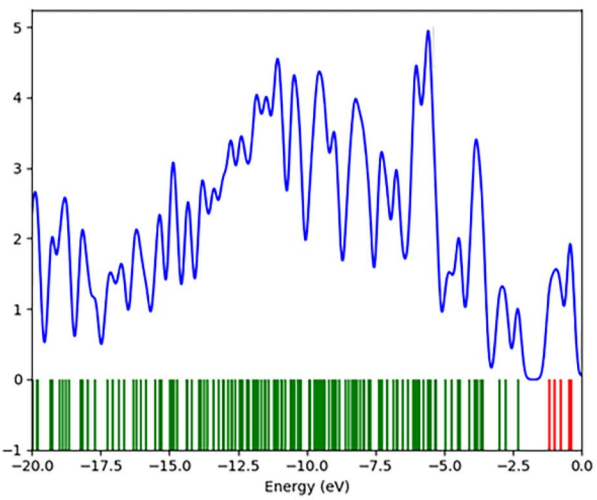

DMBMB6

Fig. 2 DOS spectra of dyes (**DMBMB1-DMBMB6**)

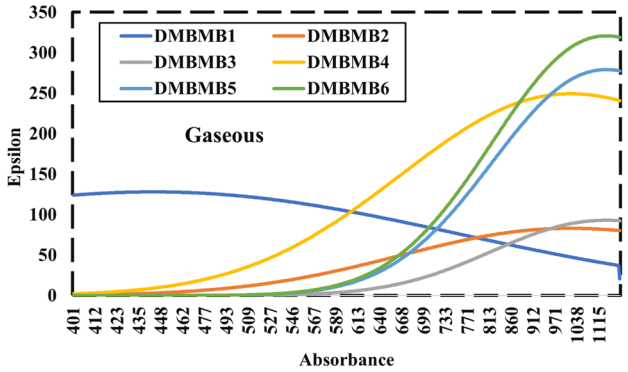

Fig. 3 Computed UV–visible spectra of dyes (**DMBMB1-DMBMB6**) in gaseous phase

such ring after excitation. Therefore, the CT feature is present in the authorized transition. A tiny singlet–triplet gap that helps relieves the thermally induced barrier to counterbalance ease of access.

Also, a powerful singlet oscillator that fabricates fluorescence around this minor barrier; and c) enhanced spin–orbit coupling that drives reverse interference crossover in this location. The abovementioned analysis has led to the opinion that the newly proposed dye molecules are more preferable to the benchmark molecule in terms of electronic and optical properties. It is believed that all of the recently created dyes have significant f^0, E, and λ_{max} values. The dyes **DMBMB3** and **DMBMB6** can therefore be used in PV devices as important non-fullerene D moieties. The novel designs of solar dyes are used for their V_{oc} values by evaluating D unit moiety for its strength as concluded by Schwarber and colleagues regarding $HOMO_D \rightarrow LUMO_A$ energy variations.

The V_{oc} measurements for newly developed dyes varied from -1.82–0.72 eV. The starting material of dye **DTB** was used as the standard electron D moiety with reference to all the dyes. All readings were negative except the dye **DMBMB6**, which was positive. The dyes **DMBMB1**-**DMBMB5** had the negative voltage suggesting an OFF position while dye

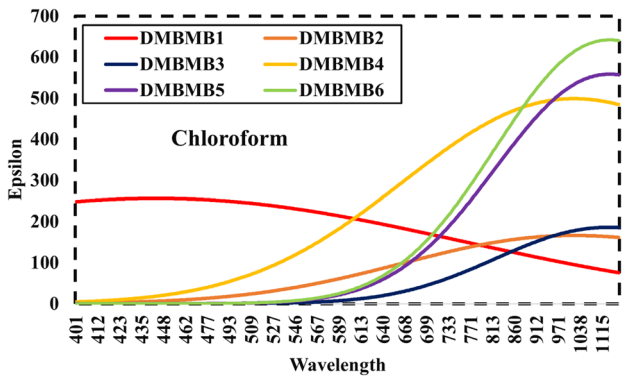

Fig. 4 Computed UV–visible spectra of dyes (**DMBMB1-DMBMB6**) in chloroform

Table 4 Absorption and other photovoltaic related parameters of dyes **DMBMB1-DMBMB6**

Dyes	E_{ge}	λ_{max}	f^0	LHE	μ_{gm}	Major Transitions (%)
DMBMB1	1.66	533	0.0036	0.124	3.12	HOMO→LUMO (73)
DMBMB2	1.28	881	0.0004	–0.713	2.12	HOMO-1→LUMO (74)
DMBMB3	1.59	835	0.0268	–0.06	1.87	HOMO-1→LUMO (82)
DMBMB4	0.39	818	0.0006	0.55	3.21	HOMO→LUMO (75)
DMBMB5	0.76	892	0.0011	0.81	2.65	HOMO→LUMO + 1 (14)
DMBMB6	0.77	856	0.0010	0.72	3.21	HOMO→LUMO (75)

DMBMB6 had the positive value for an ON position. Their V_{oc} values ranged between -1.82–0.74 eV. When utilizing **DTB** as a reference, the negative numbers proven that the flow of open-circuit voltage will act in an OFF way when **DMBMB6** was in an ON condition (Fig. 6).

Electron Injection and Hole Analysis

As (HIE = W of metal (E_{HOMO}) and (EIE = E_{LUMO}), a hole/electron injection barrier (HIE/EIE) out from dyes towards the aluminum (Al) and gold (Au) electrode is being investigated [48] as work function (W) of metal. In the HIE of novel dyes for Au metal, the declining rank was as follows: **DMBMB1** (-0.77) > **DMBMB3** (-0.93) > **DMBMB4** (-1.54) > **DMBMB6** (-1.71) > **DMBMB5** (-1.8) > **DMBMB2** (-1.88) (Table 5). It was highlighted for Al as in descending order: **DMBMB2** (3.18) > **DMBMB5**(3.16) > **DMBMB3**(3.14) > **DMBMB4** (2.99) > **DMBMB1** (2.37) > **DMBMB6** (1.71). The development for (Au) and (Al) for the dyes was also revealed some intriguing results for EIE as: **DMBMB1** (-0.49) > **DMBMB3** (-0.65) > **DMBMB4** (-1.26) > **DMBMB6** (-1.43) > **DMBMB5** (-1.52) > **DMBMB2** (-1.6). Al electrode, on the other hand, offered a very different pattern from the latter one, presenting as: **DMBMB2** (11.8) > **DMBMB5** (11.78) > **DMBMB3** (11.76) > **DMBMB4**

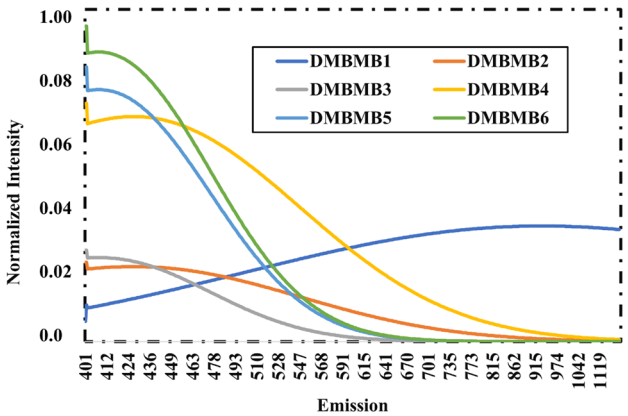

Fig. 5 Computed fluorescence spectra of dyes (**DMBMB1-DMBMB6**)

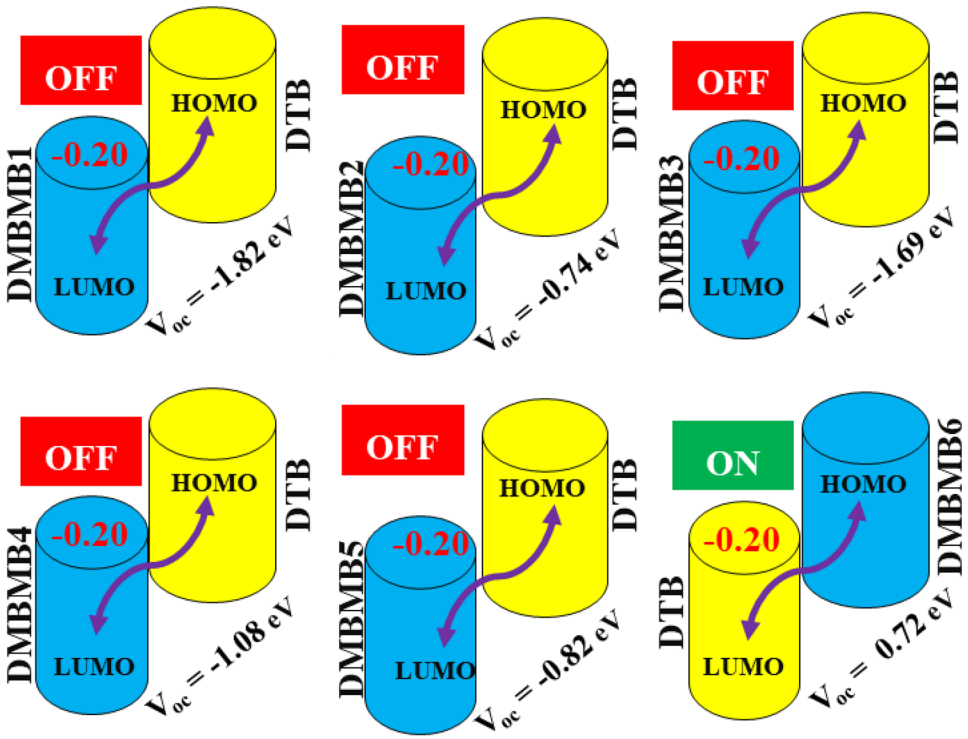

Fig. 6 Analysis of Open Circuit Voltage (V_{oc}) of dyes (**DMBMB1-DMBMB6**)

(11.61) > **DMBMB1** (10.99) > **DMBMB6** (10.33). All dyes may function as good electrochemical devices based on electron injection as well as hole investigation, and the electrode influence is almost non-existent. They also reflect a metal trend that is identical. However, it could be inferred that Au is a suitable option for electron hole research, whereas Al is an excellent electrode material during electron injection investigations.

Charge Tripping Analysis

To study the potential usage of D functionalities in OSC materials, the dye **DMBMB5**, which had a positive V_{oc} values were combined with **DTB** as a complex and optimized at B3LYP functional at its energy minima (Fig. 7). The dye **DTB** is a well-known artificial solar dye that was also commonly used in CT. To test the efficiency of charge transfer, we placed our created dyes to the D part. An established electronic environment is concentrated over dye **DMBMB6** in its HOMO; meanwhile it was concentrated over the **DTB-DMBMB6** complex including its final stage A part in LUMO. Such dyes are suitable OSCs for use in organic semiconductor applications due to the efficient flow of electrons from D to A. The approach was used to predict transition behavior, especially from the lowest energy (S_0) to an excited singlet state (S_1), as well as D-A unit exchanges with charge carrier localization. Hydrogen atoms were not included since they have such a minimal influence on such shifts.

Table 5 **HIE/EIE** analysis of newly designed dyes (**DMBMB1-DMBMB6**)

Dye	HIE (Au)	EIE(Au)	HIE (Al)	EIE (Al)
DMBMB1	2.37	–0.49	10.99	–0.77
DMBMB2	3.18	–1.60	11.80	–1.88
DMBMB3	3.14	–0.65	11.76	–0.93
DMBMB4	2.99	–1.26	11.61	–1.54
DMBMB5	3.16	–1.52	11.78	–1.80
DMBMB6	1.71	–1.43	10.33	–1.71

NLO Response

The organic materials with enough electrical connectivity across their multiple moieties have an excellent NLO response [49]. Numerous computational and experimental researchers have concentrated about material science, physics, and chemistry in research communities. As optical modulation, resonance generation, wavelength blending, and related statistics become more important, multidisciplinary attempts to develop NLO materials have been launched. To check a sequential linear relation (polarizability) and NL responses, electronic properties were employed to predict the magnitude of optical interactions (hyperpolarizabilities) computed the α_{total} and β_{total} values of the dyes that were suggested. For a comparing of the μ_{nor} and the α_{total} values,

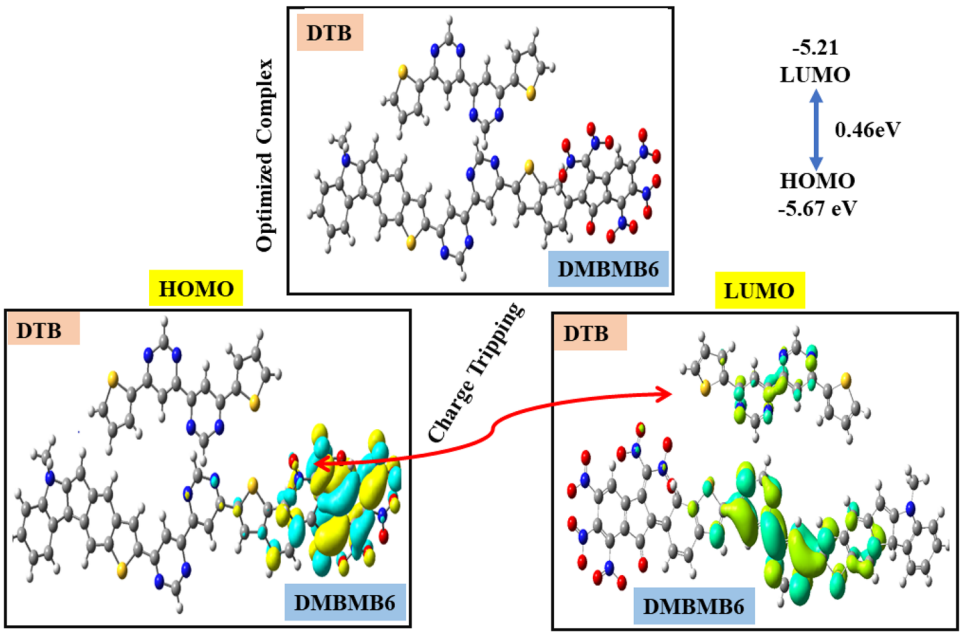

Fig. 7 Charge tripping analysis of optimized complex between dye **DMBMB6** and **DTB** at DFT level

all tensors mentioned were used as a reference material, and they have been discovered to be higher than the literature. The amount of μ_{nor} of all developed dyes was revealed to be larger than urea (1.373D). The dye **DMBMB6** had the largest μ_{nor} (8.72 D) of the all the designed dyes. The descending order of linear polarizability values noted was as: **DMBMB6** (1361.85) > **DMBMB2** (666.57) > **DMBMB5** (579.69) > **DMBMB1** (553.15) > **DMBMB3** (470.22) > **DMBMB4** (458.59). The mean polarizability of the dye **DMBMB6** was determined to be the highest (Table 6).

A remarkable increase in its value was attributed due to the presence of three nitro groups, which increased electron-withdrawing capacity by enriching the electronic structure around the A unit. The strength of substituents added to the A unit 3-dinitromethyleneindan-1-one (**A6**), affected the nonlinearity of a molecule. The conjugated system's contribution grows and becomes more dominating when replacements occur. For all proposed dyes, the β_{total} value was ordered in decreasing order: the dye **DMBMB5** was superior to dye **DMBMB6** in terms of functionality. When compared to other developed dyes, dye **DMBMB5** has the greatest overall value. Furthermore, a comparative investigation was conducted using urea as a reference part, with a total value of 714D. In compared to the reference, dye **DMBMB1** and dye **DMBMB6** had α_{total} values of 8.33 and 1.27 times higher, respectively level. The NLO response exposed is larger in **DMBMB1-DMBMB6** due to a stronger electron-withdrawing entities in the A units, which may reduce the $\mathbf{E}_{gap}$ to raise the ICT between orbitals, and render the molecule further differentiated through polarization. All suggested dyes had β_{total} values when the E_{gap} between was reversed (Fig. 8). The dye **DMBMB5** had the highest value and **DMBMB5** > **DMBMB6** > **DMBMB2** > **DMBMB3** > **DMBMB1** is the decreasing order of all the produced chemicals. For modern NLO applications, the current study delves into the intriguing NLO records of the conjugated push pull organic molecules. Furthermore, the developed dyes can be exploited as research targets due to their strong NLO response.

MEP Analysis

The electrophilic substitution positions of intended combination were revealed by molecular electrostatic potential (MEP) investigations, permitting reaction areas to be

Table 6 Second order hyperpolarizability β_{tot} of newly designed dyes (**DMBMB1-DMBMB6**) with tensor in Debye

Dyes	XXX	XYY	XZZ	YYY	YZZ	YXX	ZZZ	XXZ	XYZ	β_{total}
DMBMB1	171.2	108.1	202.1	13.2	14.2	202.4	25.2	62.3	17.6	553.15
DMBMB2	171.0	234.7	205.8	13.6	17.1	210.1	51.1	61.2	16.5	666.57
DMBMB3	101.9	81.3	187.3	16.8	18.0	221.5	23.7	63.2	45.0	470.22
DMBMB4	151.4	87.2	201.4	11.1	11.1	12.2	27.3	45.4	12.6	458.59
DMBMB5	171.9	138.9	198.5	13.0	10.2	211.2	44.9	62.6	14.6	579.69
DMBMB6	1011.6	118.7	167.3	18.6	13.7	214.8	43.2	69.2	13.2	1361.85

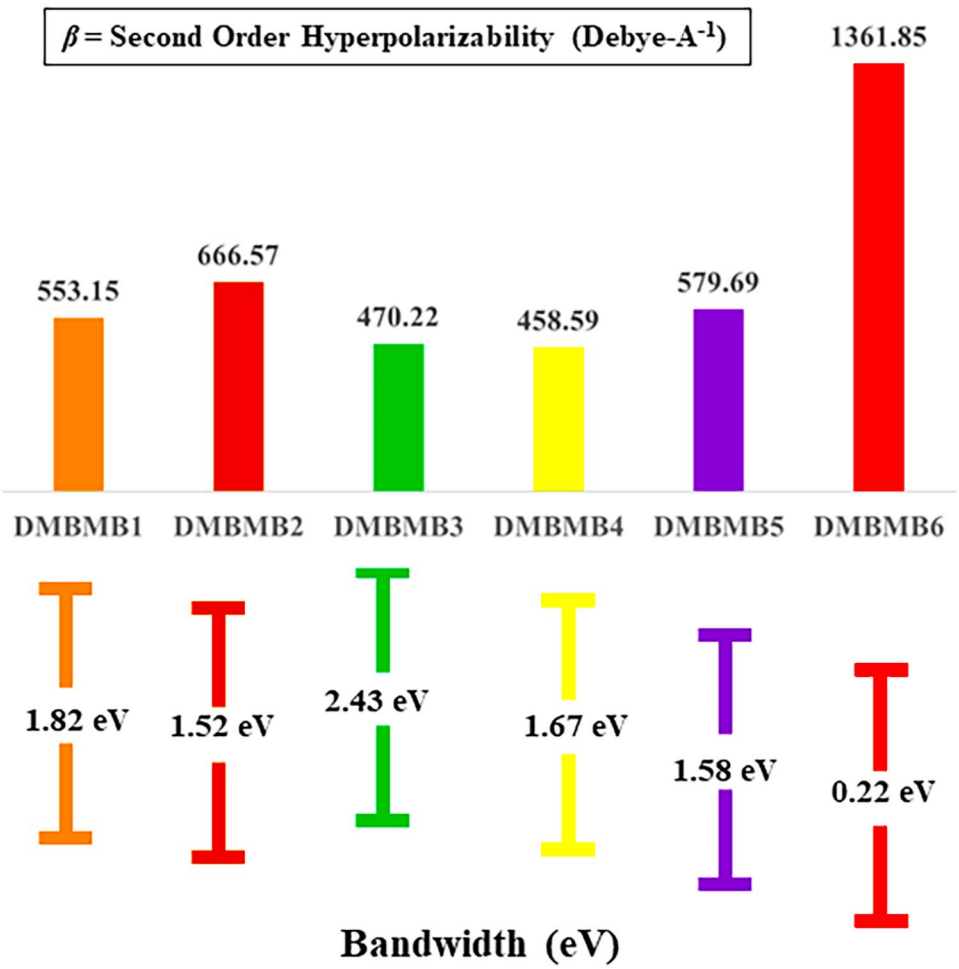

Fig. 8 Second order NLO response as unction of E_{gap} for dyes (**DMBMB1-DMBMB6**)

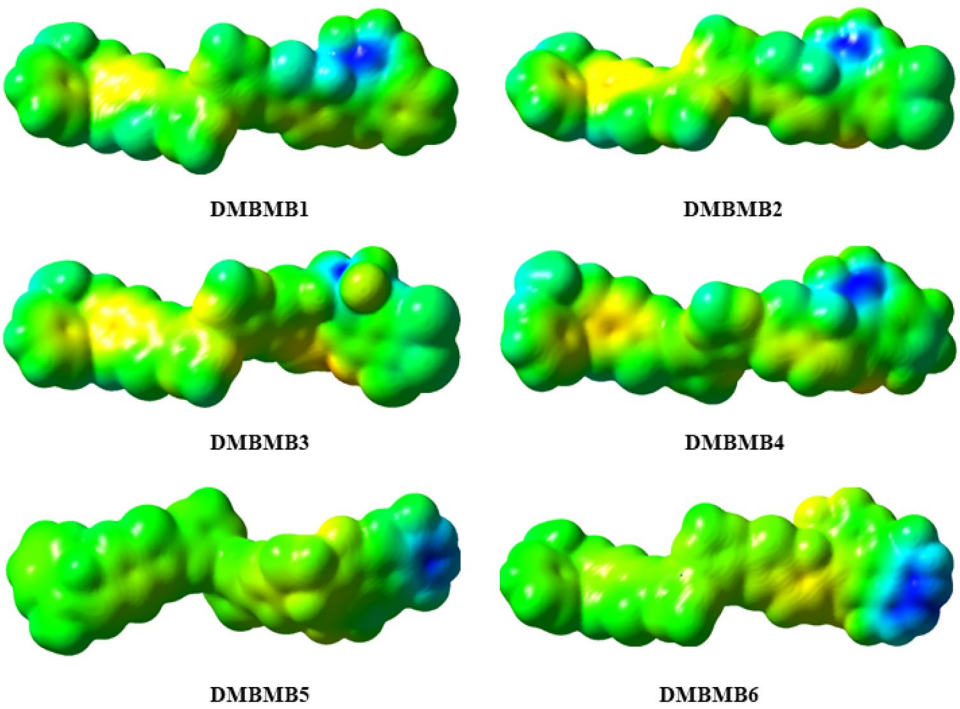

Fig. 9 MEP analysis of dyes (**DMBMB1-DMBMB6**)

predicted [50]. The red, blue, and green color reflects the negative, positive, and neutral sections of the MEP regions (Fig. 9). The negative region (red) is found mostly around electron pairs, suggesting that those places were vulnerable to electrophilic assaults [51]. The positive (blue) zone encompasses the carbon and hydrogen atoms in all dyes, suggesting that nucleophilic engagement is possible in these locations. The electrostatic energy-free areas of the dyes were known as the neutral zones.

Conclusions

By changing the various substituted functionalization, six unique organic dyes (**DMBMB1**-**DMBMB6**) were theoretically constructed from some A and D moieties with phenyl as spacers. Regarding NLO features, the effect of various A units was investigated on the either side of the dyes. The FMO measurements showed that all the developed dyes have a minute E_{gap} (0.22–2.43 eV). The GRPs were linked to a narrower E_{gap}, with lower η values and greater σ values. Furthermore, in compared to the reference molecule, all the created dyes showed higher λ_{max} readings and a lowered energy of electronic transitions in the UV–vis range (711.408 nm). Their NBO study revealed the formation of charge separation between the D and A species in molecules. Because of charge transfer from D to A, this charge separation might be the source of a large NLO reaction. The dyes **DMBMB1**-**DMBMB6** with their α_{total} values are eight times more than the reference compound. Across all newly designed dyes, **DMBMB6** generated the maximum second order NLO action, implying that this dye framework could be a suitable contender for experimental synthesis. These advancements may function as the groundwork for the wide recognition of DSSCs for energy harvesting process due to their attractive character traits such as low cost, facile synthesis with high performance.

Supplementary Information The online version contains supplementary material available at https://doi.org/10.1007/s10895-022-03075-1.

Acknowledgements The authors are grateful to the University of Gujrat, Gujrat, Pakistan for accessing the all-research facilities.

Author Contributions Conceptualization: [**Abrar U. Hassan**]; Methodology: [**Abrar U. Hassan**]; Formal analysis and investigation: [**Sajjad H. Sumrra** and **Muhammad F. Nazar**]; Writing-original draft preparation: [**Abrar U. Hassan**]; Writing-review and editing: [**Sajjad H. Sumrra**]; Resources: [**C. Guleruz**].

Funding The authors declare that no funds, grants, or other support were received during the preparation of this manuscript.

Data Availability All data generated or analyzed during this study are included in this published article and its supplementary information file.

Code Availability Gaussian 09 W and Gauss view 5.1 are used for simulation and origin software is used to draw the plots.

Declarations

Ethics Approval Not applicable.

Consent to Participate This article does not contain any studies with human participants or animals, clinical trial registration or plant reproducibility performed by any author.

Consent for Publication All authors have approved the paper and agree with its publication.

Research Involving Human and Animal Participants This work did not involve any human subjects.

Competing Interests The authors have no competing interests to declare that are relevant to the content of this article.

References

1. Erdem M, Korkmaz E, Kösouglu G et al (2021) Nonlinear optical behavior and optical power limiting characteristics of peripheral symmetrical and non-symmetrical zinc phthalocyanines with nanosecond pulsed excitation. Polyhedron 195:114975
2. Kurutos A, Citterio D (2022) Synthesis and spectral properties of near-infrared cyanine dyes showing enhanced Stokes shift: A paradigm of ICT dipolar state polymethine chromophoric systems. J Mol Struct 1247:131381
3. Ilina K, MacCuaig WM, Laramie M et al (2019) Squaraine dyes: molecular design for different applications and remaining challenges. Bioconjug Chem 31:194–213
4. Hassan AU, Sumrra SH (2022) Exploration of pull–push effect for novel photovoltaic dyes with A–π–D design: a DFT/TD-DFT investigation. J Fluoresc. https://doi.org/10.1007/s10895-022-03003-3
5. Luo X, Li J, Zhao J et al (2019) A general approach to the design of high-performance near-infrared (NIR) D-π-A type fluorescent dyes. Chin Chem Lett 30:839–846
6. Bassan E, Gualandi A, Cozzi PG, Ceroni P (2021) Design of BODIPY dyes as triplet photosensitizers: electronic properties tailored for solar energy conversion, photoredox catalysis and photodynamic therapy. Chem Sci 12:6607–6628
7. Srivishnu KS, Prasanthkumar S, Giribabu L (2021) Cu(II/I) redox couples: potential alternatives to traditional electrolytes for dye-sensitized solar cells. Mater Adv 2:1229–1247
8. Yu J, Cui Y, Wu C et al (2012) Second-order nonlinear optical activity induced by ordered dipolar chromophores confined in the pores of an anionic metal–organic framework. Angew Chemie 124:10694–10697
9. Hug W, Wagniere G (1972) The optical activity of chromophores of symmetry C2. Tetrahedron 28:1241–1248
10. Yao H, Miki K, Nishida N et al (2005) Large optical activity of gold nanocluster enantiomers induced by a pair of optically active penicillamines. J Am Chem Soc 127:15536–15543
11. Angiolini L, Benelli T, Bicciocchi E et al (2012) Synthesis and photoresponsive behavior of optically active methacrylic homopolymers containing side-chain spiropyran chromophores. React Funct Polym 72:469–477
12. Nemoto N, Miyata F, Nagase Y et al (1996) Novel types of polyesters containing second-order nonlinear optically active chromophores with high density. Macromolecules 29:2365–2371

13. Kaur S, Kaur M, Kaur P et al (2017) Ferrocene chromophores continue to inspire. Fine-tuning and switching of the second-order nonlinear optical response. Coord Chem Rev 343:185–219
14. Fominykh OD, Kalinin AA, Sharipova SM et al (2018) Composite materials containing chromophores with 3, 7-(di) vinylquinoxalinone π-electron bridge doped into PMMA: Atomistic modeling and measurements of quadratic nonlinear optical activity. Dye Pigment 158:131–141
15. Traskovskis K, Mihailovs I, Tokmakovs A et al (2012) Triphenyl moieties as building blocks for obtaining molecular glasses with nonlinear optical activity. J Mater Chem 22:11268–11276
16. Doistau B, Jiménez J-R, Piguet C (2020) Beyond chiral organic (p-block) chromophores for circularly polarized luminescence: the success of d-block and f-block chiral complexes. Front Chem 8:555
17. Muruganandi G, Raj MBJ (2019) Second and third-order NLO response of 2-amino-5-nitropyridinium tetrafluoroborate. Optik (Stuttg) 182:755–760
18. Gokila G, Aarthi R, Ramachandra Raja C (2020) Structural, spectral and nonlinear optical analysis of Sodium bis (2-methyllactato) borate: a new semiorganic crystal for photonic applications. Opt Quantum Electron 52:1–11
19. Byer RL (1994) New material for high average power infrared generation: QPM-DB GaAs. STANFORD UNIV CA EDWARD L GINZTON LAB OF PHYSICS, 1994:ADA276389
20. Aronson LB (1992) High-density integrated-optical switch arrays based on dynamic waveguide gratings. Stanford University ProQuest Dissertations Publishing, 1992:9302167
21. Abudurusuli A, Li J, Pan S (2021) A review on the recently developed promising infrared nonlinear optical materials. Dalt Trans 50:3155–3160
22. Ye J-T, Qiu Y-Q (2021) The inspiration and challenge for through-space charge transfer architecture: from thermally activated delayed fluorescence to non-linear optical properties. Phys Chem Chem Phys 23:15881–15898
23. Yahya M, Nural Y, Seferoğlu Z (2022) Recent advances in the nonlinear optical (NLO) properties of phthalocyanines: A review. Dye Pigment 198:109960
24. Zhang S, Ocheje MU, Huang L et al (2019) The critical role of electron-donating thiophene groups on the mechanical and thermal properties of donor–acceptor semiconducting polymers. Adv Electron Mater 5:1800899
25. Woo S-J, Kim Y, Kwon S-K et al (2019) Phenazasiline/spiroacridine donor combined with methyl-substituted linkers for efficient deep blue thermally activated delayed fluorescence Emitters. ACS Appl Mater Interfaces 11:7199–7207
26. Prabu S, Palanisami N (2022) Aggregation induced emission (AIE)-active ferrocene conjugated linear π- extended multi donor- π-acceptor (DD′-π-A) chromophores: Synthesis, structural, theoretical, linear and nonlinear optical studies. Dye Pigment 201:110193
27. Armin A, Li W, Sandberg OJ et al (2021) A history and perspective of non-fullerene electron acceptors for organic solar cells. Adv Energy Mater 11:2003570
28. Cheng P, Li G, Zhan X, Yang Y (2018) Next-generation organic photovoltaics based on non-fullerene acceptors. Nat Photonics 12:131–142
29. Hassan AU, Sumrra SH, Zubair M et al (2022) Structurally modulated D-π-D-A(semiconductor) anchoring dyes to enhance the tunable NLO response: a DFT/TDDFT quest for new photovoltaic materials. Struct Chem. https://doi.org/10.1007/s11224-022-02070-3
30. Liu J, Bao S, Wang X (2022) Applications of graphene-based materials in sensors: A review. Micromachines 13:184
31. Wang S, Li L, Yu S et al (2021) A review of advances in EDCs and PhACs removal by nanofiltration: Mechanisms, impact factors and the influence of organic matter. Chem Eng J 406:126722
32. Sumrra SH, Hassan AU, Imran M et al (2020) Synthesis, characterization, and biological screening of metal complexes of novel sulfonamide derivatives: Experimental and theoretical analysis of sulfonamide crystal. Appl Organomet Chem. https://doi.org/10.1002/aoc.5623
33. Frisch MJ, Trucks GW, Schlegel HB et al (2016) G16_C01. Gaussian 16, revision C.01, Gaussian, Inc., Wallin
34. Alemán C, Curcó D, Casanovas J (2005) Reliability of the density functional approximation to describe the charge transfer and electrostatic complexes involved in the modeling of organic conducting polymers. Phys Rev E 72:26704
35. Eng J, Laidlaw BA, Penfold TJ (2019) On the geometry dependence of tuned-range separated hybrid functionals. J Comput Chem 40:2191–2199
36. Trindle C (2003) DFT Studies of Biarylcarbenes and the Carbene–Biradical Continuum. J Org Chem 68:9669–9677. https://doi.org/10.1021/jo034753q
37. Hassan AU, Mohyuddin A, Güleryüz C et al (2022) Novel pull–push organic switches with D–π–A structural designs: computational design of star shape organic materials. Struct Chem. https://doi.org/10.1007/s11224-022-01983-3
38. Hassan AU, Guleryuz C (2021) Theoretical evaluation of the permeability for doscharge item (LiOOH) IN Li-O-2 batteries. Lat Am Appl Res 51:153–157
39. Sumrra SH, Arshad Z, Zafar W et al (2022) Metal incorporated aminothiazole-derived compounds: synthesis, density function theory analysis, in vitro antibacterial and antioxidant evaluation. R Soc Open Sci 8:210910. https://doi.org/10.1098/rsos.210910
40. Li W, Xie H, Huang Y et al (2016) Application of Gaussian 09/GaussView 5.0 in analytical chemistry teaching. J Kunming Med Univ 134–136
41. Hanwell MD, Curtis DE, Lonie DC et al (2012) Avogadro: an advanced semantic chemical editor, visualization, and analysis platform. J Cheminform 4:17. https://doi.org/10.1186/1758-2946-4-17
42. Zhurko GA, Zhurko DA (2009) ChemCraft, version 1.6. https://www.chemcraftprog.com
43. Singh Y, Patel RN, Patel SK et al (2019) Experimental and quantum computational study of two new bridged copper (II) coordination complexes as possible models for antioxidant superoxide dismutase: Molecular structures, X-band electron paramagnetic spectra and cryogenic magnetic properties. Polyhedron 171:155–171. https://doi.org/10.1016/j.poly.2019.07.015
44. De Angelis F, Fantacci S, Selloni A et al (2010) First-principles modeling of the adsorption geometry and electronic structure of Ru (II) dyes on extended TiO2 substrates for dye-sensitized solar cell applications. J Phys Chem C 114:6054–6061. https://doi.org/10.1021/jp911663k
45. Hassan AU, Mohyuddin A, Nadeem S et al (2022) Structural and electronic (absorption and fluorescence) properties of a stable triplet diphenylcarbene: A DFT study. J Fluoresc. https://doi.org/10.1007/s10895-022-02969-4
46. Sumrra SH, Hassan AU, Zafar MN et al (2022) Metal incorporated sulfonamides as promising multidrug targets: Combined enzyme inhibitory, antimicrobial, antioxidant and theoretical exploration. J Mol Struct 1250:131710. https://doi.org/10.1016/j.molstruc.2021.131710
47. Mintmire JW, White CT (1998) Universal density of states for carbon nanotubes. Phys Rev Lett 81:2506
48. Hassan AU, Sumrra SH, Zafar MN et al (2022) New organosulfur metallic compounds as potent drugs: synthesis, molecular modeling, spectral, antimicrobial, drug likeness and DFT analysis. Mol Divers 26:51–72. https://doi.org/10.1007/s11030-020-10157-4
49. Noreen S, Sumrra SH (2022) Correlating the charge transfer efficiency of metallic sulfa-isatins to design efficient NLO materials

with better drug designs. Biometals. https://doi.org/10.1007/s10534-022-00385-6
50. Hassan AU, Sumrra SH, Imran M, Chohan ZH (2022) New 3d multifunctional metal chelates of sulfonamide: spectral, vibrational, molecular modeling, DFT, medicinal and in silico studies. J Mol Struct 132305. https://doi.org/10.1016/j.molstruc.2021.132305
51. Hassan AU, Sumrra SH (2022) Exploring the bioactive sites of new sulfonamide metal chelates for multi drug resistance: An experimental versus theoretical design. J Inorg Organomet Polym Mater 32:513–535. https://doi.org/10.1007/s10904-021-02135-6